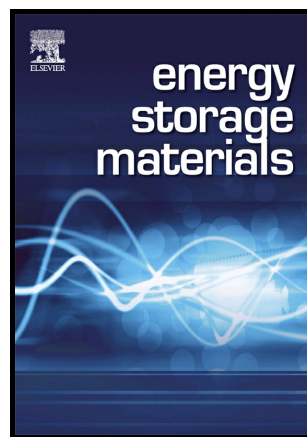


Author's Accepted Manuscript

Structural and Mechanistic Revelations on High Capacity Cation-disordered Li-rich Oxides for Rechargeable Li-ion Batteries

Enyue Zhao, Lunhua He, Baotian Wang, Xiyang Li, Junrong Zhang, Yang Wu, Jie Chen, Shaoying Zhang, Tianjiao Liang, Yuanbo Chen, Xiqian Yu, Hong Li, Liquan Chen, Xuejie Huang, Hesheng Chen, Fangwei Wang



www.elsevier.com/locate/ensm

PII: S2405-8297(18)30415-X
DOI: <https://doi.org/10.1016/j.ensm.2018.06.016>
Reference: ENSM426

To appear in: *Energy Storage Materials*

Received date: 9 April 2018
Revised date: 29 May 2018
Accepted date: 14 June 2018

Cite this article as: Enyue Zhao, Lunhua He, Baotian Wang, Xiyang Li, Junrong Zhang, Yang Wu, Jie Chen, Shaoying Zhang, Tianjiao Liang, Yuanbo Chen, Xiqian Yu, Hong Li, Liquan Chen, Xuejie Huang, Hesheng Chen and Fangwei Wang, Structural and Mechanistic Revelations on High Capacity Cation-disordered Li-rich Oxides for Rechargeable Li-ion Batteries, *Energy Storage Materials*, <https://doi.org/10.1016/j.ensm.2018.06.016>

This is a PDF file of an unedited manuscript that has been accepted for publication. As a service to our customers we are providing this early version of the manuscript. The manuscript will undergo copyediting, typesetting, and review of the resulting galley proof before it is published in its final citable form. Please note that during the production process errors may be discovered which could affect the content, and all legal disclaimers that apply to the journal pertain.

Structural and Mechanistic Revelations on High Capacity Cation-disordered Li-rich Oxides for Rechargeable Li-ion Batteries

Enyue Zhao^{1,2}, Lunhua He^{1,3}, Baotian Wang^{3,4}, Xiyang Li^{1,2}, Junrong Zhang^{3,4}, Yang Wu^{3,4}, Jie Chen^{3,4}, Shaoying Zhang^{1,3}, Tianjiao Liang^{3,4}, Yuanbo Chen^{3,4}, Xiqian Yu^{1,2,*}, Hong Li^{1,2,*}, Liquan Chen^{1,2}, Xuejie Huang^{1,2}, Hesheng Chen^{3,4} and Fangwei Wang^{1,2,3*}

¹Beijing National Laboratory for Condensed Matter Physics, Institute of Physics, Chinese Academy of Sciences, Beijing 100190, China

²School of Physical Sciences, University of Chinese Academy of Sciences, Beijing 101408, China

³Dongguan Neutron Science Center, Dongguan 523808, China

⁴Institute of High Energy Physics (IHEP), Chinese Academy of Sciences, Beijing 100049, China

X.Y. (xyu@iphy.ac.cn)

H.L. (hli@iphy.ac.cn)

F.W. (fwwang@iphy.ac.cn)

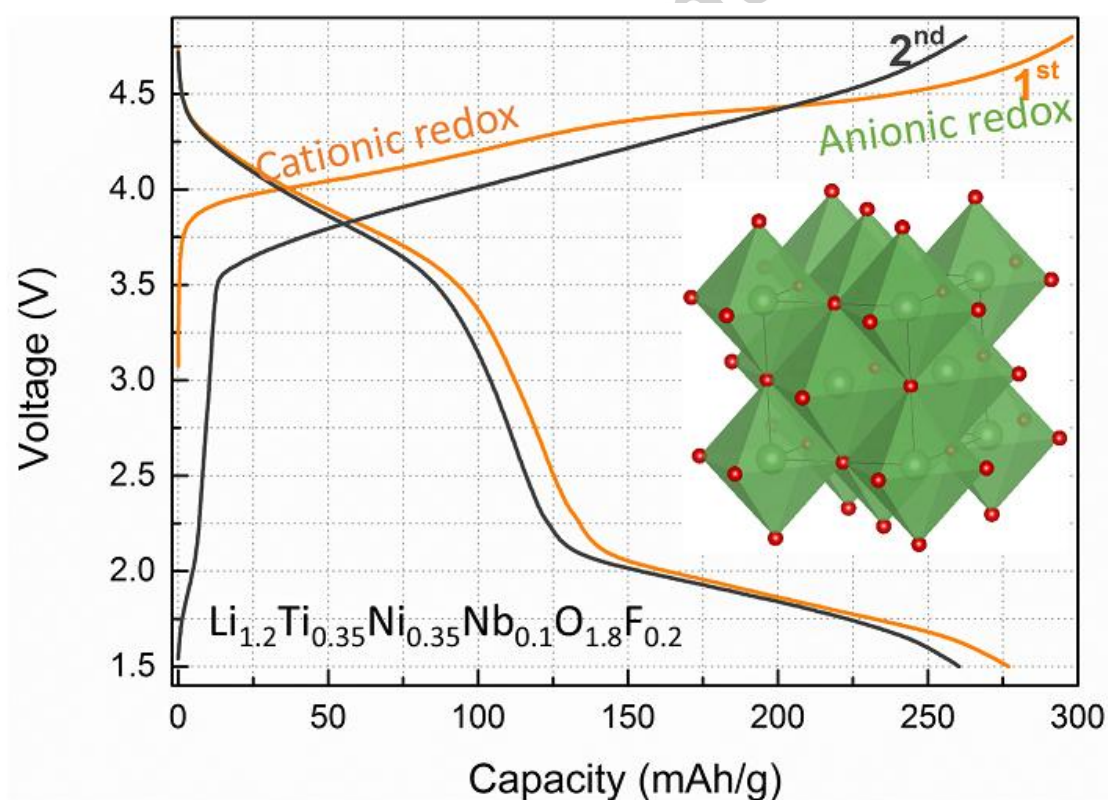
*Corresponding authors.

Abstract

High capacity cation-disordered Li-rich oxides not only enlarge the chemical design space of cathode materials, but also play an important role in promoting the development of high energy density Li-ion batteries. However, there are still some issues, such as capacity degradation, that impede their practical applications. In-depth understanding of the structure and mechanisms in cation-disordered Li-rich oxides is favorable for their further performance optimization. Herein, taking the new designed high capacity (~280 mAh/g) disordered $\text{Li}_{1.2}\text{Ti}_{0.35}\text{Ni}_{0.35}\text{Nb}_{0.1}\text{O}_{1.8}\text{F}_{0.2}$ as a model

compound, we meticulously study its structure evolution and electrochemical reaction mechanisms upon cycling by combination of first principles calculation, synchrony X-ray diffraction (SXRD), X-ray pair distribution function (XPDF), X-ray absorption spectroscopy (XAS), in situ XRD, and Neutron powder diffraction (NPD) et al. The excellent structure stability and robust anions framework of cation-disordered Li-rich oxides are experimentally demonstrated. Meanwhile, the high capacity mechanisms rely on the simultaneous cations and anions redox reactions and the capacity degradation mechanism induced by oxygen loss upon cycling are also proposed. Based on these revelations, the optimization strategy and potential applications of cation-disordered Li-rich oxides are further proposed.

Graphical abstract



Keywords: Cathode, cation disorder, lithium-rich oxide, lithium-ion batteries

1. Introduction

Rechargeable Li-ion batteries have facilitated the rapid progress of portable electronics and are considered as the technology of choice for electric vehicles as well as smart grid[1-4]. Higher energy density is required for Li-ion batteries to better satisfy large-scale applications. At present, ordered layered Li transition metal (TM) oxides have dominated the cathode markets due to their advantages of high capacity [5-7]. In these ordered compounds, Li layers are separated from the TM layers by oxygen forming 2D Li pathways between the bonded TMO_2 layers. The conventional wisdom is that the well-ordered structure is favorable for layered cathodes to achieve good performance[8, 9]. Based on this standpoint and early electrochemical inactive results verified in disordered Li compounds (e.g. $\gamma\text{-LiFeO}_2$), passion and efforts to explore as well as to develop cation-disordered cathode materials, in which Li and TMs share the same sublattice, are inherently limited[10, 11].

Encouragingly, Ceder et al. unlocked the potential of cation-disordered cathode materials for Li-ion batteries. They pointed out that an excess of Li over TM of at least 10% is an essential prerequisite for Li transport or forming percolating active O-TM network in cation-disordered oxides[12, 13]. With this percolation theory of guidance, several new high-capacity Li-rich cathodes with cation-disordered rocksalt structure had been designed and showed great advantage in specific capacity[14-21]. Unquestionably, the development of cation-disordered Li-rich oxides enlarges the chemical design space for high-capacity Li-ion battery cathodes. More importantly, cation-disordered Li-rich oxides own considerable advantages over traditional layered cathodes. For instance, cations disorder was suggested to be favorable for the structural stability and immutability of Li^+ local environment upon Li (de)intercalation[12, 13]. The excess Li (vs. TM) coupled with 3D Li channels in these cation-disordered oxides make it possible to achieve high-energy and high-power densities for Li-ion batteries[12, 13].

However, till now, almost all the reported cation-disordered cathodes are hindered by factors, such as inferior cycle stability, large polarization, voltage degradation and etc., from practical applications. Nonetheless, these issues will not bankrupt the potential of cation-disordered oxides for high-energy density candidate cathodes. Just like layered Li- and Mn-rich oxides, which have numerous issues at the beginning of development, whereas many drawbacks of them have been effectively overcome after years of efforts[22-25]. It should be noted that a good understanding of cation-disordered oxides is the premise of improving their performance. Recently, the effects of cation disorder on the voltage profile and average Li intercalation voltage were understood in the research conducted by Ceder's group[26, 27]. To more effectively ameliorate developed cation-disordered oxides and broaden their application prospect, an in-depth insight of the characters of their structure and electrochemical performance appear to be urgent and significant.

With this motivation in mind, the central goal of this work is to better understand the structure and mechanisms in cation-disordered Li-rich oxides, further providing effective strategies or guidelines for their optimization and design. Meanwhile, the in-depth and systematic understanding in cation-disordered oxides are hoped to spark more thoughts with different aspects on their application prospects. To achieve the above objectives, $\text{Li}_{1.2}\text{Ti}_{0.35}\text{Ni}_{0.35}\text{Nb}_{0.1}\text{O}_{1.8}\text{F}_{0.2}$ (LTNNbOF) with superior reversible capacity (energy density) of 280 mA h/g (750 W h/Kg), a new cation-disordered Li-rich cathode designed for the first time, was selected as the model compound. Multiple characterization techniques (e.g. SXRD, XAS, TOF NPD, X-ray PDF, etc.) combined with first-principle calculation are used to study its (local & average) structure evolution upon cycling, redox reaction behaviors, surface/interface chemistry and Li-ion migration thermodynamics/kinetics, etc. The research results demonstrate the excellent structure stability of high capacity cation-disordered LTNNbOF cathode upon long cycles and highlight its application potential. More importantly, the insightful understanding provides a clear and instructional path towards optimizing/designing cation-disordered oxides with superior electrochemical performance in the future and paves the way for the development of high energy

density rechargeable Li-ion batteries.

2. Experimental section

2.1 Materials Synthesis

All the cation-disordered Li-rich oxides were prepared by a solid-state reaction using precursor of Li_2CO_3 (100 %, Alfa), TiO_2 (99.8%, Alfa), and NiCO_3 (98 %, Alfa) and Nb_2O_5 (99.5%, Alfa). Other than for $\text{LiNi}_{0.5}\text{Ti}_{0.5}\text{O}_2$, a stoichiometric amount of precursors were used. For $\text{LiNi}_{0.5}\text{Ti}_{0.5}\text{O}_2$, 5% excess Li precursor and 4% excess Ni precursor were used[14]. The precursors were dispersed into alcohol and ball milled for 15 hours and then dried in an oven. The mixed precursors were then pressed into a pellet under a pressure of 10 MPa, and the pellets were heated at 750 °C (heating rate of 5°C /min) for 2 h in air atmosphere and cooled to room temperature naturally. Chemical delithiation LTNNbOF was prepared by chemical oxidation of LTNNbOF using nitronium tetrafluoroborate NO_2BF_4 (Aldrich > 95%) as an oxidizing agent[28]. A two-fold excess of NO_2BF_4 was dissolved in acetonitrile before adding the LTNNbOF powder, and stirred for 16 h under Ar gas protection. Then the mixture was filtered and washed several times with acetonitrile before drying the oxidized powder under vacuum.

2.2 Materials Characterization

Laboratory XRD, Scanning Electron Microscopy (SEM), Transmission Electron Microscopy (TEM) and XPS

The structure was characterized using an X'Pert Pro MPD X-ray diffractometer (D8 Bruker) with Cu-K α radiation in the scan range (2θ) of 10°-120°. The morphologies of the samples were investigated by SEM (Hitachi-S4800) and TEM (FEI Tecnai G2 F20). In the in situ XRD studies, the working electrode was prepared using polyvinylidene fluoride (PVDF) as binder on an Al foil. A specially designed Swagelok cell equipped with an X-ray-transparent aluminum window was used for the in situ measurements. The in situ XRD patterns were collected with an interval of 30 min for each 2θ scan from 35° to 50° and 60° to 66° on charge and discharge at 20 mA/g, between 1.5 and 4.8 V versus Li/Li⁺. For all ex situ characterizations, the cells

were disassembled at different states of charge and discharge, and the cathode was washed three times in DMC before drying, assembled in an argon-filled glove-box. The XPS spectra were recorded with a spectrometer having Mg/Al K_{α} radiation (ESCALAB 250 Xi, Thermo Fisher). All binding energies reported were calibrated using the signal of the Super P at 284.4 eV as an internal standard. All samples were protected from air and moved to the detector cavity by the transfer equipment provided by Thermo Fisher.

Synchrotron XRD/PDF, XAS and NPD

Synchrotron X-ray diffraction experiments were carried out at beamline 17-BM-B ($\lambda = 0.24129 \text{ \AA}$) at the Advanced Photon Source (APS) in Argonne National Laboratory. X-ray total scattering experiments were carried out at the X-ray powder diffraction (XPD) beamline (28-ID-2) at the National Synchrotron Light Source II (NSLS-II, Brookhaven National Laboratory, USA), with a photon wavelength of 0.185794 \AA . The diffraction patterns collected from the two-dimensional detector were radially integrated using Fit2D[29]. The pair distribution functions, $G(r)$, were extracted using PDFgetX3[30]. XAS data were collected in transmission mode at beamline BL14W at Shanghai Synchrotron Radiation Facility (SSRF) and 12-BM-B at the Advanced Photon Source (APS) in Argonne National Laboratory. NPD data were collected at the beamline of general purpose powder diffractometer (GPPD) at the Chinese Spallation Neutron Source (CSNS). Refinement of the SXRD, NPD and XPDF data were carried out using programs of FullProf[31] and PDFgui[29], respectively.

2.3 Electrochemical Measurements

All the electrochemical tests were conducted using coin cells (CR2032), assembled in an argon-filled glove-box. The cathodes were prepared by mixing 70 wt% of active material, 20 wt% of acetylene black as an electronic conductor, and 10 wt% of polyvinylidene fluoride binder (PVDF) in N-Methyl pyrrolidone (NMP). The slurry was deposited on an aluminum plate and drying at $120 \text{ }^{\circ}\text{C}$ in vacuum for 10 h. The electrolyte was 1 mol/L LiPF_6 in a 1:1 mixture of ethylene carbonate (EC)/dimethyl carbonate (DMC) and the separator was Celgard 2500. The galvanostatic

charge-discharge tests were carried out using a Land CT2001A battery test system (Land, Wuhan, China) in a voltage range of 1.5-4.8 V at various C-rates at room temperature. The potentiostatic intermittent titration technique (PITT) measurements were performed on an electrochemical station (Metrohm-Autolab, PGSTAT 302N). Electrochemical impedance spectroscopy (EIS) measurements were measured at an open-circuit voltage in the frequency range of 8 MHz to 100 mHz on an electrochemical station (CHI600E).

2.4 Calculation methods

First-principles calculations were performed on the cation-disordered $\text{LiTi}_{0.5}\text{Ni}_{0.5}\text{O}_2$ and $\text{Li}_{1.2}\text{Ti}_{0.6}\text{Ni}_{0.2}\text{O}_2$ to better understand the effect of TM environments on the Li diffusion properties. In order to compare to the experimental results, a $2 \times 2 \times 2$ super cells containing 64 atoms was built by the special quasi-random structure (SQS) approach[32]. The special SQS approach proposed by Zunger et al. can closely mimic the most relevant local pair and multisite correlation functions of the random substitutional alloys. DFT calculations were performed by using the Vienna ab initio simulation package (VASP)[33] with the Perdew–Burke–Ernzerhof approximation as the exchange–correlation functional. The cutoff energy of plane wave was set to 500 eV, and the k-mesh of $3 \times 3 \times 3$ was used in integrating the Brillouin zone. These settings turn out to be sufficient to obtain electronic convergence to less than 1.0×10^{-6} eV[34]. The migration energy barriers of Li ions were calculated using the climbing image nudged elastic band (CI-NEB) method[35].

3. Results

3.1 The design idea and structure of cation-disordered Li-rich oxides

To provide an in-depth understanding for cation-disordered cathode materials, we designed a series of Li-rich disordered compounds on the basis of disordered host material $\text{LiTi}_{0.5}\text{Ni}_{0.5}\text{O}_2$ (LTNO)[36]. The new disordered oxides were designed to contain 20 % excess lithium, and thus to obtain 0-TM diffusion channels based on the percolation theory. To balance the charge of excess lithium and reduce the loss of nickel ($\text{Ni}^{2+/4+}$ redox capacity) as much as possible, two possible schemes can be

adopted: doping cationic ions with higher valence than Ti^{4+} at TM sites or doping anionic ions with higher valence than O^{2-} at oxygen site. In view of the effect of weight and size of substitution ions on the specific capacity and preparation of compounds, we purposefully select pentvalence Nb and minus monovalence F as the substitution atoms to synthesize disordered Li-rich oxides. The theoretical specific capacity of these new designed cation-disordered Li-rich compounds is shown in Figure SI 1. It can be seen that $\text{Li}_{1.2}\text{Ti}_{0.4}\text{Ni}_{0.4}\text{O}_{1.6}\text{F}_{0.4}$ (LTNOF) compound displays the advantage of theoretical specific capacity due to the more content of Ni and less formula weight.

Lab X-ray diffraction (XRD) results (Figure SI 2) suggest that both Li-rich LTNOF and $\text{Li}_{1.2}\text{Ti}_{0.35}\text{Ni}_{0.35}\text{Nb}_{0.1}\text{O}_{1.8}\text{F}_{0.2}$ (LTNNbOF) oxides present pure phase, whereas, it is difficult for $\text{Li}_{1.2}\text{Ti}_{0.3}\text{Ni}_{0.3}\text{Nb}_{0.2}\text{O}_2$ to achieve single phase. The reason may be that super abundant niobium ions are not favorable for the formation of solid solution. The morphology information of the prepared disordered samples can be seen in Figure SI 3-5. The disordered cubic rocksalt structure with a space group of Fm-3m of LTNOF and LTNNbOF compounds are demonstrated by Rietveld refinement of SXRD data (Figure SI 6, Figure 1a and Table SI 1-3). Taking an example of LTNNbOF, the disordered rocksalt structure can be simply described as that all the cations distribute randomly on the cationic sublattice (4a Wyckoff sites), while O^{2-} and F^- distribute randomly on the anionic sublattice (4b Wyckoff sites)[14, 36] (Figure 1b).

In addition, to probe the local structure of cation-disordered oxides, X-ray total scattering technique, including Bragg and diffuse scattering, combined with atomic PDF method was used to provide the short-range and intermediate-range structure information. As shown in Figure 1c and Figure SI 7a, the average Rietveld structure of LTNNbOF obtained from the refinement result of SXRD (Figure 1a) was used as the initial model to fit the PDF file at different r range, and overall all the PDF peaks can be well fitted. It is worth noting that the refined residual (R_w) increases with the reduction of r range, Figure SI 7a I to V, suggesting that the local structure of LTNNbOF is not consistent with its average structure. The variation of the refinement

cell parameters from SXRD and different r range PDF file is illustrated in Figure SI 7b, in which it can be seen that the bond distance ($4a_{\text{atom}}-4b_{\text{atom}}$) obtained from the average PDF file (1.6-30 Å) is basically consistent with that obtained from the SXRD patterns. Also, the bond length slightly increases with the reduction of r range (Figure SI 7b I-IV).

Another point should be noted is that the refined residual (R_w) will significantly decrease when we only focused on the first PDF peak (Figure SI 7a V), which indicates that the first atom coordination environment in LTNNbOF can be well simulated by Fm-3m space group, and the corresponding cell parameters is much different from other files (Figure SI 7a V). The deviation between the original and refined PDF file (e.g. $4a-4a$ vs. r_2) in Figure 1c indicates that there is local distortion in the real structure of LTNNbOF, which can only be probed by total scattering. Moreover, a unique shoulder peak located at about 2.48 Å (r^2) cannot be successfully fitted using crystal structure units, suggesting the existence of short-range structure in LTNNbOF. Similar results can also be observed in the disordered LTNO and LTNOF oxides (Figure SI 8, 9). The analysis of the LTNO and LTNOF PDF files, effects of the substitution on the PDF file, as well as the corresponding detailed results are illustrated in the supporting information. (Figure SI 10)

3.2 Electrochemical performances and Li-ion migration thermodynamics for cation-disordered Li-rich oxides

The electrochemical performances of cation-disordered Li-rich LTNOF and LTNNbOF cathodes were detected in a half cell at 20 mA/g between 1.5-4.8 V. As displayed in Figure SI 11, the initial charged capacity of LTNOF cathode is only about 189 mA h/g, which does not show much advantage in capacity compared with that of electrochemical inert LTNO. Although the excess Li in LTNOF can theoretically form the percolating network of 0-TM Li channels, its specific capacity does not meet the expected theoretical value. The phenomenon indicates that the (de)intercalation process of Li^+ in LTNOF may be determined by many other factors (e.g. limited electronic conductivity, etc.), and further works are required to clear it[36, 37].

Excitingly, the LTNNbOF cathode shows superior electrochemical behaviors, the

first charged capacity of which is up to about 300 mA h/g (equivalent to extraction of about 1.0 Li). (Table SI 4) In addition, the first Columbic efficiency (CE) of LTNNbOF compound can reach up to $\approx 94\%$ which is higher than that of reported Li- and Mn-rich layered cathodes (Figure 2a). Both of the ultrahigh specific capacity and excellent CE make Li-rich LTNNbOF oxide more competitive to be a candidate cathode for high energy density Li-ion batteries. Moreover, the potential of cycle stability (Figure 2b) and good rate capability (Figure 2c) of Li-rich LTNNbOF cathode are also worthy of attention. The variation of polarization and Li⁺-ions migration kinetics of LTNNbOF upon cycling process were clearly displayed by the PITT results in Figure 2d.

In order to explore the effect of Li⁺ local environments on its diffusion thermodynamics, disordered LiTi_{0.5}Ni_{0.5}O₂ with 2-TM channels and disordered Li-rich Li_{1.2}Ti_{0.6}Ni_{0.2}O₂ with 0-TM channels were selected as the research models (Figure 3). As shown in Figure 3c, the calculated Li⁺ diffusion energy barrier is 0.94 eV for the LiTi_{0.5}Ni_{0.5}O₂ model and 0.56 eV for the Li_{1.2}Ti_{0.6}Ni_{0.2}O₂ model, respectively. According to the Arrhenius equation, the diffusion coefficient (D) of Li follow $D = \exp(-E/kBT)$, which means that the diffusion velocity of Li in 0-TM local environment is much faster than that in 2-TM local environment. The results further confirm that the 0-TM Li⁺ local environment is favorable for the migration of Li⁺ from one octahedra to another one in cation-disordered oxides.

3.3 Redox reaction mechanisms for cation-disordered Li-rich oxides

It is notable in Figure 2a that the capacity of LTNNbOF exceeds its theoretical Ni²⁺/Ni⁴⁺ capacity (214 mA h/g), which suggests that not only Ni²⁺/Ni⁴⁺ but also other redox couples are active in LTNNbOF. Usually, Ni²⁺ is oxidized to Ni^{3+/4+} in LTNNbOF during the charging process, and the ionic radius of Ni³⁺ ($r = 0.56 \text{ \AA}$) and Ni⁴⁺ ($r = 0.48 \text{ \AA}$) is smaller than that of Ni²⁺ ($r = 0.69 \text{ \AA}$). The oxidation of Ni²⁺/Ni^{3+/4+} upon charging process will result in the change of cell parameters of LTNNbOF. Accordingly, we firstly used in situ lab XRD to study the redox reaction behaviors in LTNNbOF. Here, we focused on the evolution trend of the Bragg peaks upon the charging process. As shown in Figure 4a, the Bragg peaks (shadow region)

drastically shift to high 2θ angle at the starting charging process (< 4.2 V) and the shift becomes slower upon the subsequent charging process (4.2 - 4.5 V), then almost no shift at the end of the charging process (> 4.5 V). The evolution results of Bragg peaks position further verify that there is not only Ni^{2+} participate in the charge compensation in LTNNbOF upon the charging process. Specifically, it can be inferred that the drastically shift of Bragg peaks may be correlated with the oxidation of Ni^{2+} , and the slow shift of peaks may be ascribed to the oxidation of lattice oxygen, which can shrink the oxygen framework in LTNNbOF either by making the oxygen ion smaller in size or by introducing peroxy-like species whose O-O bond distance is shorter. The relative stable cell parameters at the end of the charging process may be attribute to the charge compensation by oxygen loss, since the oxygen loss will slow down the increase in the oxidation states of the remaining ions in LTNNbOF [14, 38-40]. SXRD refinement results of the 4.55 V charged and 4.8 V charged samples also indicate that the oxygen loss mainly occurred at the end of the charging process. (Figure SI 12 and Table SI 5, 6)

Furthermore, X-ray absorption near edge spectroscopy (XANES) measurements were performed to study the electronic structure of TMs in LTNNbOF upon cycling process. Figure 4b and 4c show the different electrochemical states Ni K-edge and Nb K-edge XANES spectra of LTNNbOF, respectively. It can be seen in Figure 4b that the Ni K-edge shifts to higher energy during the first charge to 4.5 V, and then barely shifts during the subsequent charge to 4.8 V. The results confirm the above standpoints obtained from in situ XRD that the simultaneous oxidation of cationic ions (Ni^{2+}) and anionic ions (O^{2-}) provides the charge compensation for Li^+ deintercalation in LTNNbOF upon the first charging process. Upon the first discharging process, the Ni edge returns to its starting position, indicating the excellently reversible redox reactions of Ni ions. Since Nb is already at its high valence state, we only pay attention on the change of the Nb K-edge upon discharging process. As shown in Figure 4c, there is a little shifting of the Nb K-edge to low energy after discharged to 1.5 V, which means that there may be charge-compensation from reduction of Nb ions upon discharging process. It should be noted is that the

pre-edge peak of Nb K-edge XANES at about 18995 eV increases in intensity after the first cycling process. It has been reported that the intensity of the pre-edge peak increases as the site symmetry of the TM ions decreases from a centrosymmetric to a non-centrosymmetric environment[41, 42]. The intensity increase of Nb pre-edge peak of LTNNbOF implies that the Nb environment deviates from the regular octahedral coordination upon cycling, which may originate from a distortion of the Nb–O octahedra induced by the redox reaction of oxygen. For Ti^{4+} ions, it will not be oxidized in LTNNbOF upon the charging process [14, 43] and more experiment work is needed to further confirm the redox reaction of Ti ions upon the discharging process.

Overall, it can be concluded that the storage of charge in LTNNbOF during the first charging process is provided by the oxidation of Ni^{2+} , oxidation of oxygen ions, and oxygen loss. In addition, according to the previous reported Ni K-edge XANES results, the Ni^{2+} in LTNNbOF is not fully oxidized (i.e., oxidized to Ni^{4+}) during the first charging process[44, 45]. The competition between TMs and oxygen redox has been reported in many Li-rich oxides. Usually, there is Li-O-Li configuration in Li-rich oxides, and the O 2p orbitals along which do not have a metal orbital to hybridize with and do not hybridize with the Li 2s orbital either due to the large energy difference between the O 2p and Li 2s orbitals[46, 47]. Therefore, there will be orphaned unhybridized O 2p states in the Li-O-Li configuration, and the energy levels of which is higher than that of the hybridized O bonding states (Figure 4d). The existed orphaned unhybridized O 2p bands and its overlap with e_g^* bands ($\text{Ni}^{2+}/\text{Ni}^{4+}$) may be responsible for the not fully oxidized Ni^{2+} in LTNNbOF upon the charging process[46, 47]. From the above, it can be suggested that the full utilization of TMs and the reversible oxygen redox reactions are of importance for the disordered oxides with excellent performance.

3.4 Structure and surface chemistry evolution of cation-disordered Li-rich oxides upon (de)lithiation process

As mentioned above, almost all the reported cation-disordered Li-rich oxides show the challenges in long cycle life. Thus, it is necessary to probe the reasons (e.g.,

structure recession, surface impedance, etc.) that cause the capacity degradation of disordered Li-rich oxides upon long cycles. Firstly, ex situ SXRD was used to precisely understand the structural evolution of cation-disordered Li-rich oxides during Li^+ (de)intercalation as well as long cycle processes. Rietveld refinement results in Figure SI 12 suggest that no obvious phase transition occurred for LTNNbOF cathode during the first cycling process, and the structure (volume) change as a function of Li concentration is small, which will lead to less mechanical stress and is favorable for the structural stability upon subsequent cycles. (Table SI 5-7) After one cycle, there is about 0.7 % structure change for LTNNbOF, and more excitedly, an almost zero volume change (1^{st} vs. 118^{th} cycle, 0.6 %) can be seen after 118 long cycles (Figure 5a, b and Table SI 8, 9).

Ex situ PDF was further used to probe the local structure evolution of LTNNbO upon long cycles. It can be seen in Figure 5c that the weak feature peak ($r' = 2.48 \text{ \AA}$) of short-range structure existed in the pristine state becomes apparent after one electrochemical cycle between 1.5 and 4.8 V. The short-range structure originates from the existence of atoms between the first coordination and the second coordination atom pairs. Considering the higher thermal motion of Li^+ in the Li-driven cathode material, and the Li^+ (de)intercalation process in the cycle, we speculate that the increased short-range structure may be correlated with the motion of Li^+ , namely, partial Li^+ does not return to previous sites during the discharging process. The similar results obtained in the Li-excess LTNOF compound after the first cycle process further demonstrate that the formation of this short-range structure is liable in the disordered materials (Figure SI 13). Meanwhile, the distribution of atomic distances and atomic thermal motions (the width of PDF peaks) of LTNNbOF are also enlarged after the first cycle's Li^+ (de)intercalation process. The irreversible microstructure change upon the first cycle may be ascribed to the oxygen loss upon the oxidation process of oxygen. The less volume change of the 1 cycled sample between 1.5-4.5 V than that between 1.5-4.8 V also indicates the effect of oxygen loss on the irreversible structure change (Figure SI 14, Table SI 10). In addition, the excellently overlapped PDF spectrums between 1^{st} and 88^{th} cycle in Figure 5c,

suggests that the increased short- and reduced long-range structures in LTNNbOF are wonderfully reversible upon subsequent long cycles. The excellent structural stability can presumably be ascribed to the isotropy structure change of cubic disordered compound during the Li^+ (de)intercalation process. As shown in Figure 5d, e, this isotropy structure change has considerable advantages over anisotropy change existed in hexagonal layered materials, which can balance the mechanical stress, stabilize the local environment of ions and suppress the occurrence of phase transition.

Since neutrons are more sensitive to Li atoms than X-rays in the case of existence of heavy atoms, NPD was used to measure more subtle structure changes in the LTNNbOF sample upon de-lithiation process[48-50]. As shown in Table SI 11, the scattering length of cations at 4a Wyckoff sites in the LTNNbOF is much smaller than that of anions at 4b sites, which provide a favorable condition for the precise structure analysis. Specifically, at the pristine state, only cubic close packing O/F framework in the LTNNbOF can be clearly detected by neutron, and the interstitial cations in the O/F octahedra will be clearly detected with the extraction of Li. As shown in Figure 6a, in the pristine LTNNbOF structure, the calculated diffraction patterns contributed from cations is well consistent with the theoretical disordered structure. More importantly, it can be seen in Figure 6c and 6d that the anions close packing framework can be well maintained after most Li extracted from the LTNNbOF bulk structure, though there is a little increase in the isotropic thermal vibration factors of anions (Table SI 12, 13). Overall, the NPD results suggest that the anions framework in the LTNNbOF disordered structure is very robust upon the de-lithiation process.

Furthermore, EIS results show that the charge transfer resistance of LTNNbOF electrode significantly enhanced with the increase of electrochemical cycling (Figure SI 15). The detrimental side reactions on the surface of LTNNbOF electrode should be responsible for the phenomenon. Thus, ex situ XPS was used to analyze the surface/interface evolution of LTNNbOF upon the first cycle. As shown in Figure SI 16a, two strong peaks at 687.6 and 684.9 eV are observed in the F 1s spectrum, the peak at 687.6 eV is from the PVDF binder, while the 684.9 eV peak has the binding energy expected for fluoride (e.g. Li-F, TM-F). After one electrochemical cycle, the

intensity of the 684.9 eV is peak significantly enhanced, which is ascribed to the formation of LiF upon cycling[51] (Figure SI 16b). Also, for the pristine electrode, the O 1s data have peaks at 529.6 and 531.6 eV, from the oxide and carbonate, respectively. After one electrochemical cycling, two additional peaks located at about 532.5 and 533.5 eV appear in the O 1s spectrum. Generally, the 532.5 and 533.5 eV peaks are binding energies associated with the carbonyl oxygen and the oxygen bound to the alkyl group, respectively, in organic or semi-organic carbonates[52, 53]. In addition, the 531.5 eV peak corresponding to the inorganic Li_2CO_3 is also significantly enhanced after one electrochemical cycling. For the P 2p XPS spectrum, no feature peaks (136.5 eV spin-orbit split peaks,) expected for LiPF_6 or a related Li_xPF_y compound were found for the 1-cycled LTNNbOF electrode. The lower energy doublet at 134.2 ($2p_{3/2}$) and 135.0 eV arises from a P atom that is bound to a less electronegative element such as O[51, 54]. Since the 134.2 eV binding energy peak is too low for P_2O_5 (135 eV), it may correspond to a $\text{Li}_x\text{PF}_y\text{O}_z$ -type compound, such as Li_2PFO_3 , which is a major hydrolysis product of LiPF_6 [51]. Meanwhile, the evolution of P 2p spectra in Figure SI 16f indicates the phosphide formation process of LTNNbOF electrode. Overall, the ex situ XPS reveals the evolution of SEI and its main composition on the surface of the cation-disordered oxide electrode.

4. Discussion

4.1 Electrochemical degradation mechanisms

Similar to the previous reported high capacity cation disordered Li-rich oxides, our new designed high capacity disordered Li-rich LTNNbOF was not spared in the challenge of long cycle life. However, the excellent structural stability of LTNNbOF upon long cycling should not be ignored as a potential high-performance cathode material. According to the analysis results of SXRD, XPDF, NPD and EIS, the capacity degradation of LTNNbOF upon cycling can be mainly ascribed to the drastically increased surface/interface charge transfer resistance. To avoid or retard the phenomenon, it is of importance to control the continuous formation of SEI on the surface of the LTNNbOF electrode. Previous literatures have reported that, apart from

the effects of electrolyte, cell structure, etc., on the formation of SEI, the root cause of which is originated from the irreversible oxygen loss upon oxidation process of oxygen[38]. Our experiment results also confirm that there is oxygen loss in the LTNNbOF electrode during the charging process. For the oxygen loss mechanisms, two standpoints, namely oxygen vacancies or migration of under-coordinated TM ions from the surface into the bulk of the crystal structure, have been reported[55, 56]. Usually, the diffusion of TM ions into the bulk phase will increase the density of lattice, the occurrence of which is thermodynamically more favorable than that of oxygen vacancies in the lattice[55, 56]. Accordingly, it can be inferred that the surface of LTNNbOF electrode will become densification after oxygen loss. The ratio of Li/TM in this formed dense layer will reduce due to the increase of TM ions content, which is not favorable for the formation of 0-TM percolation Li^+ diffusion network. Meanwhile, our XPS measurement on the surface of the LTNNbOF electrode indicates a significant decrease in the O/TM mole ratio after the first cycling between 1.5-4.8 V (Figure SI 17 and Table SI 14). If it is assumed that there is no loss of TM content during the cycling process, to maintain the charge balance, the ratio of Li/TM would decrease on the surface layer and thus forming a disordered Li-poor dense layer, in which the Li content is well below the threshold for 0-TM percolation[12, 13]. The formed dense layer induced by the oxygen loss will impede the further diffusion of Li^+ -ions and result in the increased polarization and limited rate capability. (Figure SI 18) Although more calculation and characterization work are necessary to further clear this hypothesis, it is consistent with the increased polarization when LTNNbOF is charged above 4.5 V (Figure 2d), the threshold voltage after which oxygen loss occurs.

4.2 Optimization strategy

Taken together, the oxygen loss of LTNNbOF upon cycling is the root cause that results in the degradation of electrochemical performance. Therefore, to promote the practical application of LTNNbOF, or even these kinds of Li-rich materials, controlling the oxygen loss is important. As is well-known, electrode materials are not good oxide-ion conductor and the oxygen loss usually take place on their surface.

Accordingly, surface modification, as one effective strategy, can ameliorate the oxygen loss of the electrode to some extent, which have also been widely used in optimizing the traditional cathode materials. In addition, surface modification can also retard the surface side reactions and stabilize the surface/interface structure upon cycling.

Another strategy to regulate the oxygen loss of the electrode upon cycling is to optimize its electronic structures by doping suitable elements[57, 58]. Since the oxygen loss is originated from the oxidation of oxygen upon the charge-compensation process, it is effective to reduce the oxygen loss by maximizing the TM redox capacity and minimizing the oxygen redox capacity in these Li-rich materials. There is competition between TM and O redox reactions duo to the overlap between TM d orbitals and O 2p orbitals[46, 47]. Reducing the above orbitals' overlap is favorable for maximizing the TM redox capacity. For this purpose, on one hand, V, Cr, et al. with high-energy d states can be designed as the TM redox species to improve the energy level of the e_g^* and t_{2g} bands. On the other hand, decreasing the lattice parameters by cation-substitution can shrink the TM-O bond distance, thus increase the covalency of the TM-O bonding and the energy level of hybridized TM d states with anti-bonding characteristic (e_g^* or t_{2g})[46]. However, the sole TM redox usually cannot fully utilize the Li in the Li-rich oxides, take an example of LTNNbOF, the Ni^{2+}/Ni^{4+} redox capacity is about 214 mA h/g, which is below its theoretical capacity of 367 mA h/g assumed that all the Li are utilized. To achieve the high capacity, simultaneous utilization of TM and O redox is very necessary. It has been reported that the high TM-O covalency is favorable for the stabilization of the O^- oxidized species generated by Li-extraction from the O 2p-band[59]. Whereas, literatures have also reported that the less covalent cations can retard the oxygen loss upon oxygen oxidation process due to the oxide ions do not donate electrons out[19]. To propose more effective strategy to optimize the oxygen redox reactions and improve the overall performance of disordered Li-rich oxides, more research works are needed.

5. Conclusion

In conclusion, a new cation-disordered Li-rich oxide LTNNbOF with high specific capacity of 300 mAh/g was successfully designed. PITT and first-principle calculation results suggest that the cation-disordered Li-rich oxide shows excellent Li^+ -ions migration kinetics and thermodynamics. The redox reaction behaviors of LTNNbOF were studied by in situ XRD and ex situ XAS, a simultaneous cations and anions charge-compensation mechanism was proposed for its high capacity. Meanwhile, the structure and surface evolution of LTNNbOF upon cycling were detected by combination of SXRD, XPDF, NPD and XPS. The superior structure stability and robust anions framework of LTNNbOF upon (de)lithiation process were experimentally demonstrated. In addition, an electrochemical degradation mechanism induced by oxygen loss upon charging process was suggested. Based on these understandings, strategies, such as surface coating, electronic structure optimization, et al., for improving the electrochemical performance of cation-disordered Li-rich oxides were proposed. We believe that the structural and mechanistic revelations on disordered compounds will provide guidelines and spark more thoughts for the further design and optimization of high performance cathode materials.

Acknowledgements

This work is supported by the National Key R&D Program of China (2016YFA0401503), National Materials Genome Project (2016YFB0100106), National Natural Science Foundation of China (Grant No. 11675255, 51502334), Beijing Municipal Science & Technology Commission (Grants No. D171100005517001) and “Thousand Talents Program for Young Scientists” The authors are very indebted to Dr. Ping Luo and Dr. Huaile Lu, China Spallation Neutron Source (CSNS), Dongguan, China, for their help on the neutron powder diffraction experiments at GPPD. The authors are also very indebted to Dr. Xiao-Qing Yang & Enyuan Hu (Brookhaven National Laboratory) and Prof. Yong-Ning Zhou (Fudan University) for their technique help on the XAS, SXRD and XPDF experiments. The authors would like to acknowledge that the research used Beamline BL14W at Shanghai Synchrotron Radiation Facility (SSRF) and 17-BM-B and 12-BM-B at the Advanced Photon Source (Contract No. DE-AC02-06CH11357). This research

used resources 28-ID-2 of the National Synchrotron Light Source II, a U.S. Department of Energy (DOE) Office of Science User Facility operated for the DOE Office of Science by Brookhaven National Laboratory under Contract No. DE-SC0012704.

References

- [1] B. Dunn, H. Kamath, J.-M. Tarascon, Electrical energy storage for the grid: a battery of choices, *Science*, 334 (2011) 928-935.
- [2] X. Li, Y. Qiao, S. Guo, Z. Xu, H. Zhu, X. Zhang, Y. Yuan, P. He, M. Ishida, H. Zhou, Direct Visualization of the Reversible O^{2-}/O^- Redox Process in Li-Rich Cathode Materials, *Advanced Materials*, 2018 1705197-1705197.
- [3] J.B. Goodenough, K.-S. Park, The Li-ion rechargeable battery: a perspective, *Journal of the American Chemical Society*, 135 (2013) 1167-1176.
- [4] V. Etacheri, R. Marom, R. Elazari, G. Salitra, D. Aurbach, Challenges in the development of advanced Li-ion batteries: a review, *Energy & Environmental Science*, 4 (2011) 3243-3262.
- [5] B. Li, D. Xia, Anionic Redox in Rechargeable Lithium Batteries, *Advanced Materials*, 29 (2017) 1701054- 1701054.
- [6] A. Manthiram, B. Song, W. Li, A perspective on nickel-rich layered oxide cathodes for lithium-ion batteries, *Energy Storage Materials*, 6 (2017) 125-139.
- [7] J. Zhang, Q. Li, Y. Wang, J. Zheng, X. Yu, H. Li, *Energy Storage Materials*, 14 (2018) 1-7.
- [8] K.S. Kang, Y.S. Meng, J. Breger, C.P. Grey, G. Ceder, Electrodes with high power and high capacity for rechargeable lithium batteries, *Science*, 311 (2006) 977-980.
- [9] J. Breger, N. Dupre, P.J. Chupas, P.L. Lee, T. Proffen, J.B. Parise, C.P. Grey, Short- and long-range order in the positive electrode material, $Li(NiMn)_{0.5}O_2$: A joint X-ray and neutron diffraction, pair distribution function analysis and NMR study, *Journal of the American Chemical Society*, 127 (2005) 7529-7537.
- [10] R. Marom, S.F. Amalraj, N. Leifer, D. Jacob, D. Aurbach, A review of advanced and practical lithium battery materials, *Journal of Materials Chemistry*, 21 (2011) 9938-9954.
- [11] R. Kanno, T. Shirane, Y. Kawamoto, Y. Takeda, M. Takano, M. Ohashi, Y. Yamaguchi, Synthesis, structure, and electrochemical properties of a new lithium iron oxide, $LiFeO_2$, with a corrugated layer structure, *Journal of the Electrochemical Society*, 143 (1996) 2435-2442.
- [12] J. Lee, A. Urban, X. Li, D. Su, G. Hautier, G. Ceder, Unlocking the Potential of Cation-Disordered Oxides for Rechargeable Lithium Batteries, *Science*, 343 (2014) 519-522.
- [13] A. Urban, I. Matts, A. Abdellahi, G. Ceder, Computational design and preparation of cation-disordered oxides for high-energy-density Li-ion batteries, *Advanced Energy Materials*, 6 (2016) 1600488.
- [14] J. Lee, D.-H. Seo, M. Balasubramanian, N. Twu, X. Li, G. Ceder, A new class of high capacity cation-disordered oxides for rechargeable lithium batteries: Li-Ni-Ti-Mo oxides, *Energy & Environmental Science*, 8 (2015) 3255-3265.
- [15] J. Lee, J.K. Papp, R.J. Clement, S. Sallis, D.-H. Kwon, T. Shi, W. Yang, B.D. McCloskey, G.

Ceder, Mitigating oxygen loss to improve the cycling performance of high capacity cation-disordered cathode materials, *Nature Communications*, 8 (2017) 981.

[16] R. Chen, S. Ren, M. Knapp, D. Wang, R. Witter, M. Fichtner, H. Hahn, Disordered lithium-rich oxyfluoride as a stable host for enhanced Li^+ intercalation storage, *Advanced Energy Materials*, 5 (2015) 1401814.

[17] N. Yabuuchi, M. Takeuchi, M. Nakayama, H. Shiiba, M. Ogawa, K. Nakayama, T. Ohta, D. Endo, T. Ozaki, T. Inamasu, K. Sato, S. Komaba, High-capacity electrode materials for rechargeable lithium batteries: Li_3NbO_4 -based system with cation-disordered rocksalt structure, *Proceedings of the National Academy of Sciences of the United States of America*, 112 (2015) 7650-7655.

[18] M. Nakajima, N. Yabuuchi, Lithium-excess cation-disordered rocksalt-type oxide with nanoscale phase segregation: $\text{Li}_{1.25}\text{Nb}_{0.25}\text{V}_{0.5}\text{O}_2$, *Chemistry of Materials*, 29 (2017) 6927-6935.

[19] N. Yabuuchi, M. Nakayama, M. Takeuchi, S. Komaba, Y. Hashimoto, T. Mukai, H. Shiiba, K. Sato, Y. Kobayashi, A. Nakao, M. Yonemura, K. Yamanaka, K. Mitsuhashi, T. Ohta, Origin of stabilization and destabilization in solid-state redox reaction of oxide ions for lithium-ion batteries, *Nature Communications*, 7 (2016) 13814.

[20] R. Wang, X. Li, L. Liu, J. Lee, D.-H. Seo, S.-H. Bo, A. Urban, G. Ceder, A disordered rock-salt Li-excess cathode material with high capacity and substantial oxygen redox activity: $\text{Li}_{1.25}\text{Nb}_{0.25}\text{Mn}_{0.5}\text{O}_2$, *Electrochemistry Communications*, 60 (2015) 70-73.

[21] S.L. Glazier, J. Li, J. Zhou, T. Bond, J.R. Dahn, Characterization of disordered $\text{Li}_{1+x}\text{Ti}_x\text{Fe}_{1-3x}\text{O}_2$ as positive electrode materials in Li-ion batteries using percolation theory, *Chemistry of Materials*, 27 (2015) 7751-7756.

[22] M. Hu, X. Pang, Z. Zhou, Recent progress in high-voltage lithium ion batteries, *Journal of Power Sources*, 237 (2013) 229-242.

[23] H. Yu, H. Zhou, High-energy cathode materials (Li_2MnO_3 - LiMO_2) for lithium-ion batteries, *Journal of Physical Chemistry Letters*, 4 (2013) 1268-1280.

[24] E. Zhao, X. Liu, Z. Hu, L. Sun, X. Xiao, Facile synthesis and enhanced electrochemical performances of Li_2TiO_3 -coated lithium-rich layered $\text{Li}_{1.13}\text{Ni}_{0.30}\text{Mn}_{0.57}\text{O}_2$ cathode materials for lithium-ion batteries, *Journal of Power Sources*, 294 (2015) 141-149.

[25] E. Zhao, X. Liu, H. Zhao, X. Xiao, Z. Hu, Ion conducting Li_2SiO_3 -coated lithium-rich layered oxide exhibiting high rate capability and low polarization, *Chemical Communications*, 51 (2015) 9093-9096.

[26] A. Abdellahi, A. Urban, S. Dacek, G. Ceder, The effect of cation disorder on the average Li intercalation voltage of transition-metal oxides, *Chemistry of Materials*, 28 (2016) 3659-3665.

[27] A. Abdellahi, A. Urban, S. Dacek, G. Ceder, Understanding the effect of cation disorder on the voltage profile of lithium transition-metal oxides, *Chemistry of Materials*, 28 (2016) 5373-5383.

[28] S.-i. Nishimura, G. Kobayashi, K. Ohoyama, R. Kanno, M. Yashima, A. Yamada, Experimental visualization of lithium diffusion in Li_xFePO_4 , *Nature Materials*, 7 (2008) 707-711.

[29] A.P. Hammersley, S.O. Svensson, M. Hanfland, A.N. Fitch, D. Hausermann, Two-dimensional detector software: From real detector to idealised image or two-theta scan, *High Pressure Research*, 14 (1996) 235-248.

- [30] P. Juhas, T. Davis, C.L. Farrow, S.J.L. Billinge, PDFgetX3: a rapid and highly automatable program for processing powder diffraction data into total scattering pair distribution functions, *Journal of Applied Crystallography*, 46 (2013) 560-566.
- [31] J. Rodriguezcarvajal, Recent advances in magnetic-structure determination by neutron powder diffraction, *Physica B*, 192 (1993) 55-69.
- [32] A. Zunger, S.H. Wei, L.G. Ferreira, J.E. Bernard, Special quasirandom structures, *Physical Review Letters*, 65 (1990) 353-356.
- [33] G. Kresse, J. Furthmuller, Efficient iterative schemes for ab initio total-energy calculations using a plane-wave basis set, *Physical Review B*, 54 (1996) 11169-11186.
- [34] H.J. Monkhorst, J.D. Pack, Special points for Brillouin-zone integrations, *Physical Review B*, 13 (1976) 5188-5192.
- [35] G. Henkelman, B.P. Uberuaga, H. Jonsson, A climbing image nudged elastic band method for finding saddle points and minimum energy paths, *Journal of Chemical Physics*, 113 (2000) 9901-9904.
- [36] M. Kuzma, R. Dominko, A. Meden, D. Makovec, M. Bele, J. Jamnik, M. Gaberscek, Electrochemical activity of $\text{Li}_2\text{FeTiO}_4$ and $\text{Li}_2\text{MnTiO}_4$ as potential active materials for Li ion batteries: A comparison with $\text{Li}_2\text{NiTiO}_4$, *Journal of Power Sources*, 189 (2009) 81-88.
- [37] L. Zhang, H. Noguchi, D. Li, T. Muta, X. Wang, M. Yoshio, I. Taniguchi, Synthesis and electrochemistry of cubic rocksalt Li-Ni-Ti-O compounds in the phase diagram of LiNiO_2 - LiTiO_2 - $\text{LiLi}_{1/3}\text{Ti}_{2/3}\text{O}_2$, *Journal of Power Sources*, 185 (2008) 534-541.
- [38] J. Hong, H.-D. Lim, M. Lee, S.-W. Kim, H. Kim, S.-T. Oh, G.-C. Chung, K. Kang, Critical role of oxygen evolved from layered Li-excess metal oxides in lithium rechargeable batteries, *Chemistry of Materials*, 24 (2012) 2692-2697.
- [39] Z.H. Lu, J.R. Dahn, Understanding the anomalous capacity of $\text{Li}/\text{LiNi}_x\text{Li}_{1/3-2x/3}\text{Mn}_{2/3-x/3}\text{O}_2$ cells using in situ X-ray diffraction and electrochemical studies, *Journal of the Electrochemical Society*, 149 (2002) A815-A822.
- [40] D. Mohanty, S. Kalnaus, R.A. Meisner, K.J. Rhodes, J. Li, E.A. Payzant, D.L. Wood, III, C. Daniel, Structural transformation of a lithium-rich $\text{Li}_{1.2}\text{Co}_{0.1}\text{Mn}_{0.55}\text{Ni}_{0.15}\text{O}_2$ cathode during high voltage cycling resolved by in situ X-ray diffraction, *Journal of Power Sources*, 229 (2013) 239-248.
- [41] F.W. Lytle, R.B. Gregor, Discussion of X-ray-absorption near-edge structure: application to Cu in the high T_c superconductors $\text{La}_{1.8}\text{Sr}_{0.2}\text{CuO}_4$ and $\text{YBa}_2\text{Cu}_3\text{O}_7$, *Physical Review B*, 37 (1988) 1550-1562.
- [42] W.S. Yoon, C.P. Grey, M. Balasubramanian, X.Q. Yang, J. McBreen, In situ X-ray absorption spectroscopic study on $\text{LiNi}_{0.5}\text{Mn}_{0.5}\text{O}_2$ cathode material during electrochemical cycling, *Chemistry of Materials*, 15 (2003) 3161-3169.
- [43] B. Li, N. Jiang, W. Huang, H. Yan, Y. Zuo, and D. Xia, Thermodynamic Activation of Charge Transfer in Anionic Redox Process for Li-Ion Batteries, *Advanced Functional Materials*, 28 (2018) 1704864- 1704864.
- [44] E. Zhao, X. Yu, F. Wang, H. Li, High-capacity lithium-rich cathode oxides with multivalent cationic and anionic redox reactions for lithium ion batteries, *Science China-Chemistry*, 60 (2017) 1483-1493.
- [45] X. Yu, Y. Lyu, L. Gu, H. Wu, S.-M. Bak, Y. Zhou, K. Amine, S.N. Ehrlich, H. Li, K.-W. Nam, X.-Q. Yang, Understanding the rate capability of high-energy-density Li-rich layered

- $\text{Li}_{1.2}\text{Ni}_{0.15}\text{Co}_{0.1}\text{Mn}_{0.55}\text{O}_2$ Cathode Materials, *Advanced Energy Materials*, 4 (2014) 1300950.
- [46] D.-H. Seo, J. Lee, A. Urban, R. Malik, S. Kang, G. Ceder, The structural and chemical origin of the oxygen redox activity in layered and cation-disordered Li-excess cathode materials, *Nature Chemistry*, 8 (2016) 692-697.
- [47] K. Luo, M.R. Roberts, R. Hao, N. Guerrini, D.M. Pickup, Y.-S. Liu, K. Edstrom, J. Guo, A.V. Chadwick, L.C. Duda, P.G. Bruce, Charge-compensation in 3d-transition-metal-oxide intercalation cathodes through the generation of localized electron holes on oxygen, *Nature Chemistry*, 8 (2016) 684-691.
- [48] E. Zhao, L. Fang, M. Chen, D. Chen, Q. Huang, Z. Hu, Q.-b. Yan, M. Wu, X. Xiao, New insight into Li/Ni disorder in layered cathode materials for lithium ion batteries: a joint study of neutron diffraction, electrochemical kinetic analysis and first-principles calculations, *Journal of Materials Chemistry A*, 5 (2017) 1679-1686.
- [49] E. Zhao, Z. Hu, L. Xie, X. Chen, X. Xiao, X. Liu, A study of the structure-activity relationship of the electrochemical performance and Li/Ni mixing of lithium-rich materials by neutron diffraction, *RSC Advances*, 5 (2015) 31238-31244.
- [50] M. Chen, E. Zhao, D. Chen, M. Wu, S. Han, Q. Huang, L. Yang, X. Xiao, Z. Hu, Decreasing Li/Ni disorder and improving the electrochemical performances of Ni-rich $\text{LiNi}_{0.8}\text{Co}_{0.1}\text{Mn}_{0.1}\text{O}_2$ by Ca doping, *Inorganic Chemistry*, 56 (2017) 8355-8362.
- [51] A.M. Andersson, D.P. Abraham, R. Haasch, S. MacLaren, J. Liu, K. Amine, Surface characterization of electrodes from high power Lithium-ion batteries, *Journal of the Electrochemical Society*, 149 (2002) A1358-A1369.
- [52] G.R. Zhuang, Y.F. Chen, P.N. Ross, The reaction of lithium with dimethyl carbonate and diethyl carbonate in ultrahigh vacuum studies by X-ray photoemission spectroscopy, *Langmuir*, 15 (1999) 1470-1479.
- [53] G. Beamson, D. Briggs, Hi-resolution monochromated X-ray photoelectron-spectroscopy of organic polymers: a comparison between solid-state data for organic polymers and gas-phase data for small molecules, *Molecular Physics*, 76 (1992) 919-936.
- [54] K. Nagayama, K. Kamioka, E. Iwata, H. Oka, Y. Tokunaga, T. Okada, The reaction of lithium-manganese oxides for the cathode materials of rechargeable lithium batteries with nonaqueous electrolyte, *Electrochemistry*, 69 (2001) 6-9.
- [55] A.R. Armstrong, M. Holzapfel, P. Novak, C.S. Johnson, S.-H. Kang, M.M. Thackeray, P.G. Bruce, Demonstrating oxygen loss and associated structural reorganization in the lithium battery cathode $\text{Li}_{0.2}\text{Ni}_{0.2}\text{Mn}_{0.6}\text{O}_2$, *Journal of the American Chemical Society*, 128 (2006) 8694-8698.
- [56] H. Koga, L. Croguennec, M. Ménétrier, P. Mannesiez, F. Weill, C. Delmas, S. Belin, Operando X-ray absorption study of the redox processes involved upon cycling of the Li-rich layered oxide $\text{Li}_{1.20}\text{Mn}_{0.54}\text{Co}_{0.13}\text{Ni}_{0.13}\text{O}_2$ in Li ion batteries, *the Journal of Physical Chemistry C*, 118 (2014) 5700-5709.
- [57] H. Yan, B. Li, Z. Yu, W. Chu, D. Xia, First-Principles Study: Tuning the Redox Behavior of Lithium-Rich Layered Oxides by Chlorine Doping, *The Journal of Physical Chemistry C*, 121 (2017) 7155-7163.
- [58] B. Li, H. Yan, J. Ma, P. Yu, D. Xia, W. Huang, W. Chu, Z. Wu, Manipulating the Electronic Structure of Li-Rich Manganese-Based Oxide Using Polyanions: Towards Better Electrochemical Performance, *Advanced Functional Materials*, 24(2014) 5112-5118.

[59] Y. Xie, M. Saubanere, M.L. Doublet, Requirements for reversible extra-capacity in Li-rich layered oxides for Li-ion batteries, *Energy & Environmental Science*, 10 (2017) 266-274.

Accepted manuscript

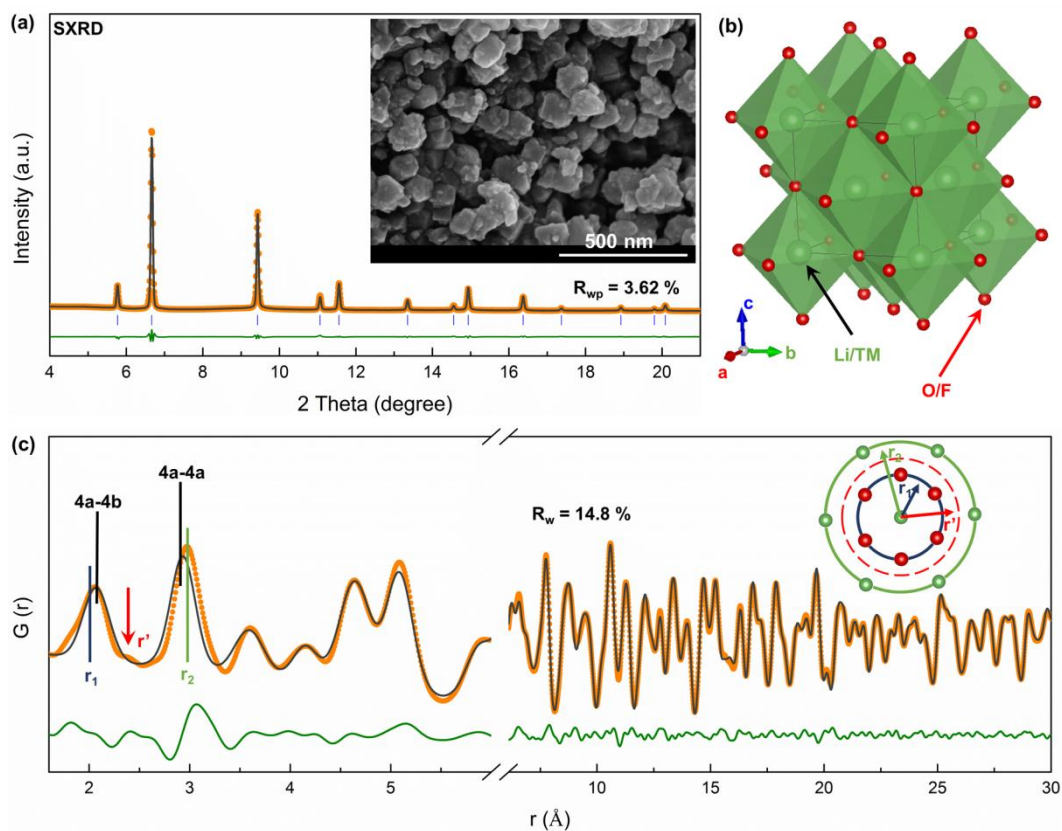


Figure 1. Crystal structure of the pristine $\text{Li}_{1.2}\text{Ti}_{0.35}\text{Ni}_{0.35}\text{Nb}_{0.1}\text{O}_{1.8}\text{F}_{0.2}$ sample. (a) Rietveld refinement of the SXR D patterns for the pristine LTNNbOF structure, insets show the SEM result; (b) The crystal structure of LTNNbOF; (c) Refinement of the X-ray PDF patterns of LTNNbOF, inset is the illustration of the congruent relationship between the PDF peaks and atomic pairs in the real space structure.

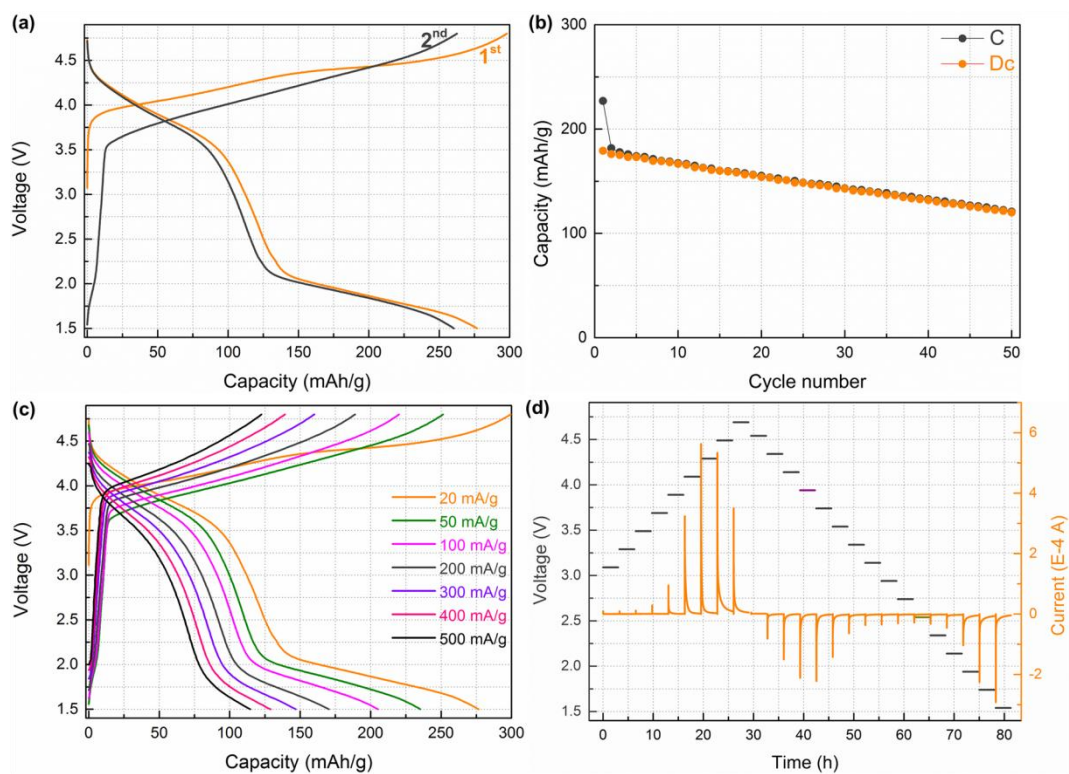


Figure 2. Electrochemical performance of the $\text{Li}_{1.2}\text{Ti}_{0.35}\text{Ni}_{0.35}\text{Nb}_{0.1}\text{O}_{1.8}\text{F}_{0.2}$ sample.

(a) The voltage profiles for the first two cycles of LTNNbOF versus Li^+/Li at 20 mA/g; (b) The capacity evolution of LTNNbOF over 50 cycles at 100 mA/g; (c) The voltage profiles of LTNNbOF when charged and discharged once at 20 mA/g, and then at 50, 100, 200, 300, 400 and 500 mA/g for the subsequent cycles [1.5–4.8 V]; (d) PITT results of LTNNbOF upon the first cycle.

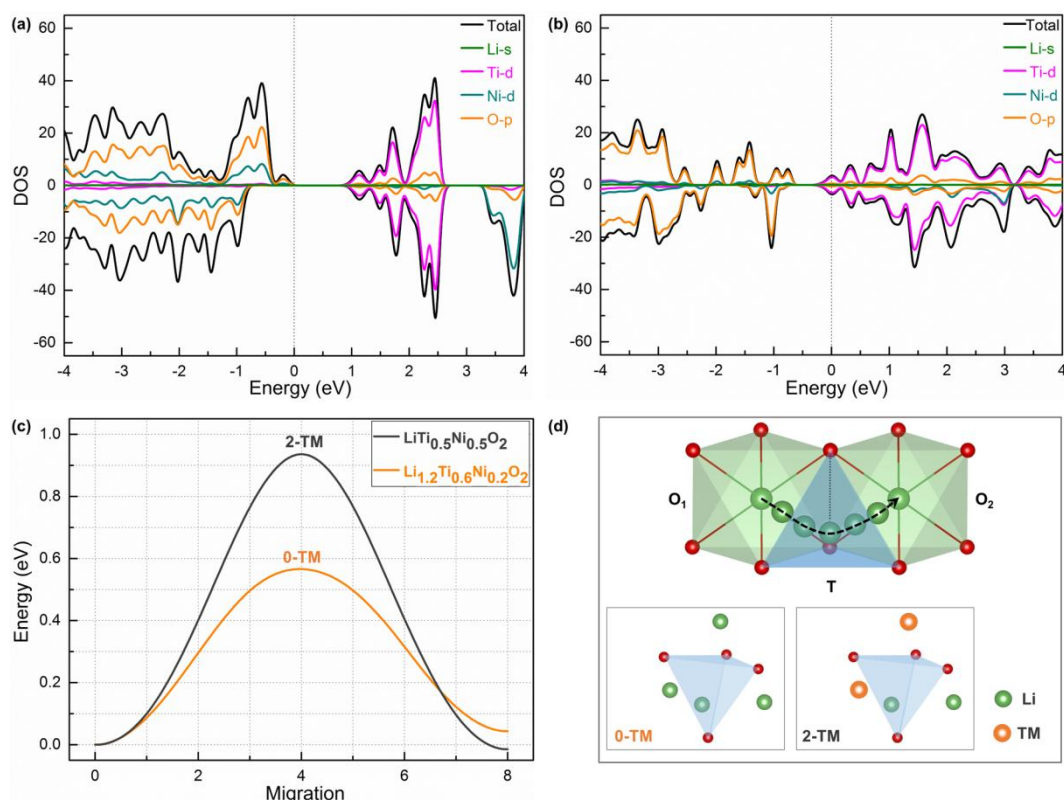


Figure 3. The calculated Li-ions diffusion energy barrier in cation-disordered Li-TM oxides. The Li-1s, Ti-3d, Ni-3d and O-2p orbital density of states in cation-disordered (a) $\text{LiTi}_{0.5}\text{Ni}_{0.5}\text{O}_2$ and (b) $\text{Li}_{1.2}\text{Ti}_{0.6}\text{Ni}_{0.2}\text{O}_2$ materials, in which the Fermi energy was set to be 0 eV. (c) The energy curves for Li-ions diffusion in cation-disordered $\text{LiTi}_{0.5}\text{Ni}_{0.5}\text{O}_2$ and $\text{Li}_{1.2}\text{Ti}_{0.6}\text{Ni}_{0.2}\text{O}_2$ materials; (d) Illustration of the Li-ions diffusion path (octahedron₁ (O_1)-tetrahedron (T)-octahedron₂ (O_2)) and schematic of two different environments for an O-T-O Li hop in cation-disordered Li-TM oxides.

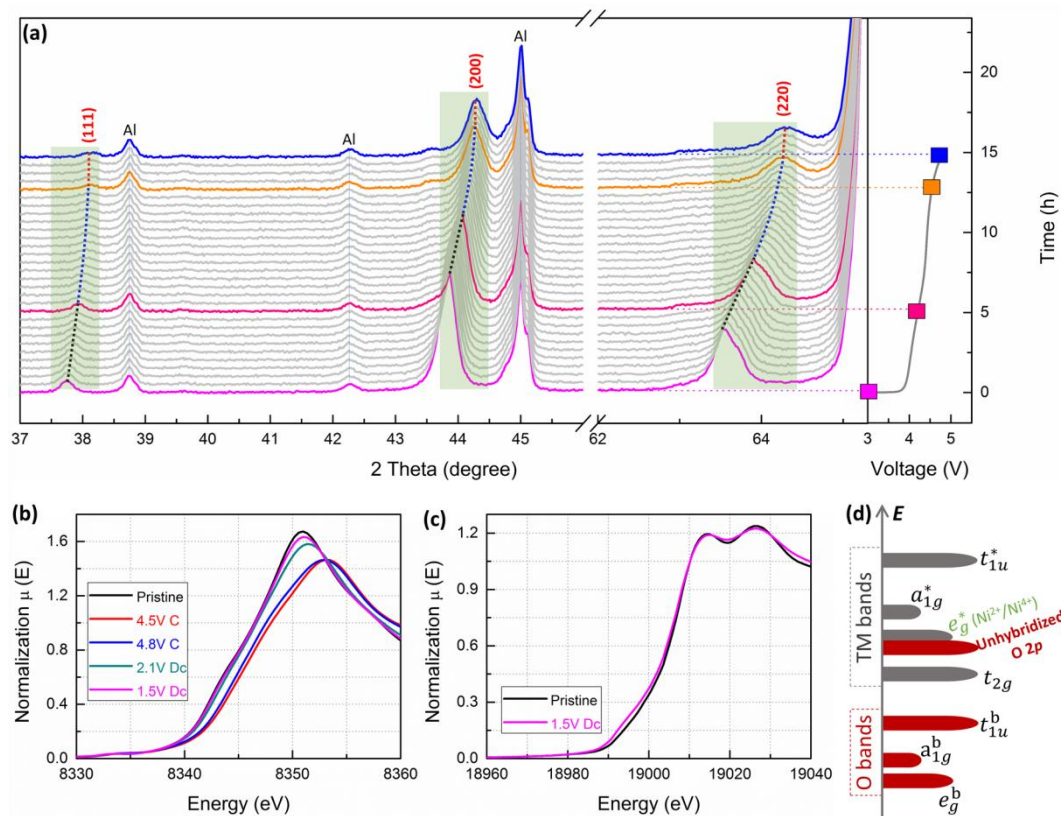


Figure 4. Redox reaction behaviors of the $\text{Li}_{1.2}\text{Ti}_{0.35}\text{Ni}_{0.35}\text{Nb}_{0.1}\text{O}_{1.8}\text{F}_{0.2}$ sample upon the first cycling process. (a) *In situ* lab XRD patterns of LTNNbOF upon the first charging process; The XANES of (b) Ni K-edge and (c) Nb K-edge in LTNNbOF at different charge-discharged states upon the first cycling process; (d) Schematic of the band structure for LTNNbOF, in which the energy of unhybridized O 2p states is higher than that of hybridized O 2p states (e_g^b , a_{1g}^b , t_{1u}^b).

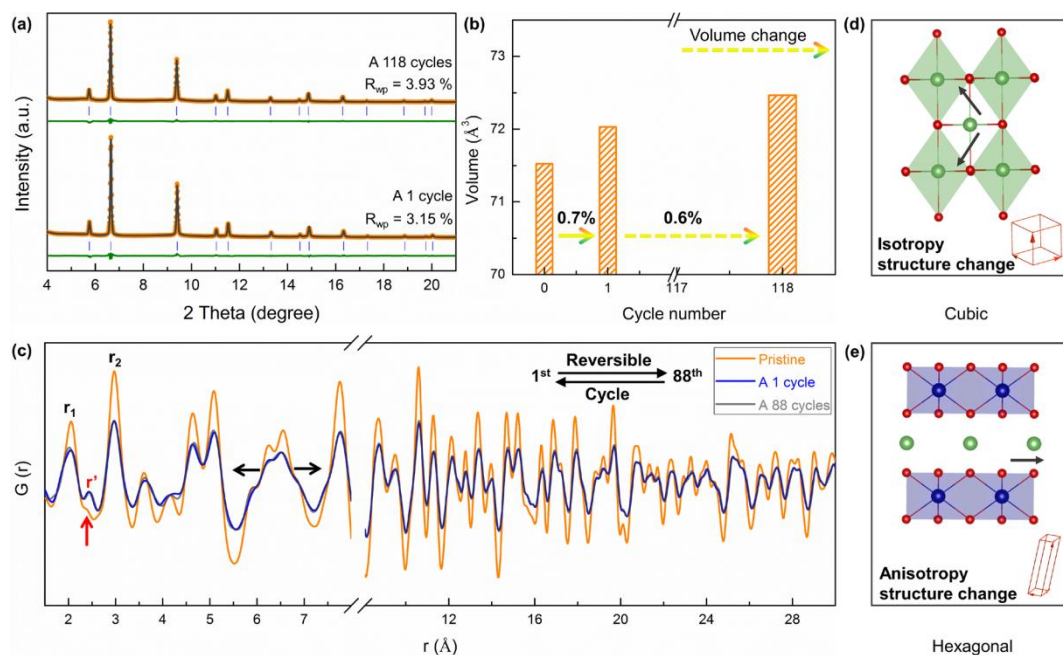


Figure 5. Structure evolution of the $\text{Li}_{1.2}\text{Ti}_{0.35}\text{Ni}_{0.35}\text{Nb}_{0.1}\text{O}_{1.8}\text{F}_{0.2}$ sample upon long cycles. (a) Rietveld refinement of the SXRD patterns for the 1-cycled and 118-cycled LTNNbOF structure; (b) The unit cell volume change of LTNNbOF upon long cycles; (c) The evolution of X-ray PDF file of LTNNbOF upon long cycles; (d, e) The comparison of structure change between cubic and hexagonal structure materials during the (de)lithiation processes.

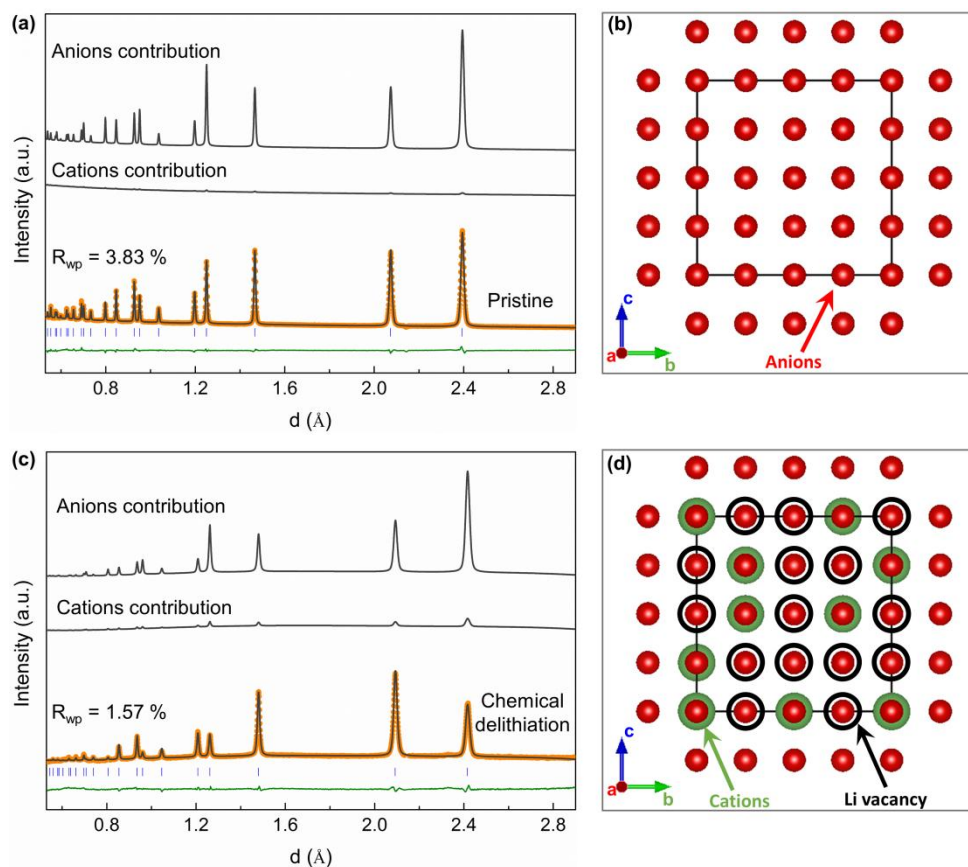


Figure 6. Detection of structural Changes upon chemical de-lithiation. Rietveld refinement of the NPD patterns and calculated cations/anions diffraction patterns for the pristine (a) and Li extracted (c) LTNNbOF structure; The corresponding schematic crystal structure detected by NPD for the pristine (b) and Li extracted (d) samples.